Talanta 217 (2020) 121080

Contents lists available at ScienceDirect

Talanta

journal homepage: www.elsevier.com/locate/talanta

An impedimetric genosensor for *Leishmania infantum* based on electrodeposited cadmium sulfide nanosheets

R. Nazari-Vanani[a], H. Heli[a,*], N. Sattarahmady[a,b,**]

[a] Nanomedicine and Nanobiology Research Center, Shiraz University of Medical Sciences, Shiraz, Iran
[b] Department of Medical Physics, School of Medicine, Shiraz University of Medical Sciences, Shiraz, Iran

ARTICLE INFO

Keywords:
Leishmaniasis
L. infantum
DNA biosensor
CdS
Nucleic acid
Electrochemical sensor

ABSTRACT

It is estimated that there are 400000 new cases of visceral leishmaniasis each year, with about 30,000 deaths. Therefore, detection of this pathogen and its species is highly vital for overall health of the community. In the present research, a DNA-based biosensor, namely genosensor, was introduced for detection of genomic DNA of *Leishmania infantum*. The genosensor was fabricated based on the transduction of cadmium sulfide nanosheets and recognition of a particular single stranded DNA sequence, and worked in label-, marker-, tag- and PCR-free manners. Impedimetric measurements were performed in a wide range of frequency (recording Nyquist diagrams) without applying external force (working at open circuit potential) upon hybridization of DNA targets with the cadmium sulfide nanosheets surface-immobilized probe. The genosensor detected the complementary DNA strand in a concentration range of 1.0×10^{-14} to 1.0×10^{-6} mol L^{-1} and a detection limit (DL) of 0.81 fmol L^{-1} (6.5 fg mL^{-1}), and genomic DNA of *Leishmania infantum* in a concentration range of 5–50 ng μL^{-1} and a DL of 1.2 ng μL^{-1}. The genosensor had a very good selectivity, fabrication reproducibility and stability, and was applicable for practical applications.

1. Introduction

DNA detection is one of focuses in biotechnology, genetic, virology, agriculture, forensic pathology, and diagnosis [1]. Oligonucleotide hybridization for DNA detection is one of the major principles of biosensors function [1,2]. This type of biosensors is a strategic alternative for development of new routes for nucleic acid analysis (including mutant gene detection) with enormous applicability in disease diagnosis with the advantages of simple, sensitive, rapid and inexpensive response generation mechanism(s), and can be miniaturized, making it suitable for field testing [1–4]. DNA biosensors use various types of transducers including metals, carbon and semiconductors [2–5], and various types of probe immobilization routes including adsorption, covalent binding, and entrapment [2–6].

Nanomaterials have exhibited substantial advantages in development of biosensors [2–5,7–9]. It is because they demonstrate special electrical, optical and catalytic activities. These activities originate from the quantum size that can be changed with size and shape. Nanostructures can be synthesized with various types of shapes and sizes by electrochemical deposition [2,9,10], and have been applied to various fields of nanomedicine, environment engineering, biological analysis and biosensors [2,9–11]. Recently, there have been attentions about synthesis of novel nanostructures for electrochemical DNA biosensing [2–5]. Among the more profitable nanomaterials, semiconductor nanostructures appear as basic elements in biosensors. Different nanostructures of semiconductors such as titanium oxide, cadmium sulfide, cadmium selenide, cadmium telluride and zinc oxide have been used for biosensors fabrication [11]. As one of the well known semiconductors, cadmium sulfide has the capability of binding to polymers, proteins, ions and nanoparticles [12–15], and applications in multiplexed assays from immunoassays to DNA analysis [16].

Leishmaniasis as a widespread infectious disease is caused by the *Leishmania* parasites, and transmitted by vectors of phlebotomine sand fly species of the genera *Lutzomyia* in the New World and Phlebotomus in the Old one [17]. Visceral leishmaniasis (VL) as one of the most severe clinical manifestations of leishmaniasis, is caused by the species of *Leishmania infantum* (*L. infantum*) parasite that can cause a high rate of mortality. In VL, *L. infantum* parasite migrates to the visceral organs of bone marrow, spleen and liver [18]. As the main host of *L. infantum*, dogs are considered as the primary reservoirs for human Leishmania infections [19]. Clinical presentation in this host is characterized by renal alterations, prolonged fever, splenomegaly, hepatomegaly, ocular

* Corresponding author.
** Corresponding author. Nanomedicine and Nanobiology Research Center, Shiraz University of Medical Sciences, Shiraz, Iran.
E-mail addresses: hheli7@yahoo.com, heli@sums.ac.ir (H. Heli), sattarahmady@yahoo.com, nsattar@sums.ac.ir (N. Sattarahmady).

https://doi.org/10.1016/j.talanta.2020.121080
Received 1 December 2019; Received in revised form 25 March 2020; Accepted 22 April 2020
Available online 29 April 2020
0039-9140/

lesions, skin disease, and respiratory system and cardiovascular disorders. It is estimated that there are > 400000 new cases of VL each year with > 40000 deaths [20]. Hence, early and accurate diagnosis and proper management of *L. infantum* infection is highly important. In addition, accurate and simple tests are needed to identify treatment failures [21]. Generally, leishmaniasis is confirmed by (i) amastigotes presence by microscopic recognition; (ii) detection of the parasite genomic DNA in tissue samples; (iii) enzyme-linked immunosorbent assay (ELISA); (iv) indirect immunofluorescence assay test (IFAT); and (v) detection of the parasite reproductive form in the spleen aspirates or bone marrow [22,23]. Although these methods can be considered for VL diagnosis and can bring reliable results, specific limitations have been found for these methods [23]. Therefore, new methods of simple biosensing of *L. infantum* are needed.

Several sensing methods for detection of *Leishmania* parasites have been reported. An electrochemical biosensor for *L. infantum* detection was presented [24]. It was based on the immobilization of a DNA probe sequence on gold surface covered with a layer of a polyaniline matrix with a terminal thiol group (PANIAuNp). The probe-parasite DNA binding was followed by impedance spectroscopy and cyclic voltammetry. Also, polymerase chain reaction (PCR) was explored for *L. infantum* detection [25–27]. Sensitivity of this technique for *L. infantum* diagnosis in the canine blood was 0.1 fg of DNA [27]. An immunosensor based on surface plasmon resonance (SPR) was developed using a thiol-modified gold chip in which positive canine serum showed a significant variation in SPR angle [28]. Western blot (WB), IFAT and ELISA, as serological tests, were frequently used for diagnosis of clinical feline leishmaniasis [29]. Median sensitivity of these methods was 0.97, 0.75 and 0.70, and median specificity was 0.99, 0.97 and 0.98 for WB, IFAT and ELISA, respectively. IFAT was more sensitive and ELISA was better for diagnosis of clinical leishmaniasis. In another study, a transducer composed of thiolated carbon nanotubes (ThNTs) was fabricated for detection of *Leishmania* spp in a femtomolar level. DNA by impedance spectroscopy [30]. The sensor represented linear responses for parasite DNA in a range of 0.1–98.3 fg μL^{-1}.

In the present study, fabrication and evaluation of a genosensor for quantitation of *L. infantum* genomic DNA were reported. Cadmium sulfide nanosheets (CSN) were prepared in two steps of electrodeposition followed by chemical conversion, and employed as a transducer. Detection was performed by impedimetry without using label, marker, tag or PCR amplification. The genosensor was successfully applied for clinical samples.

2. Material and methods

2.1. Chemicals

The employed chemicals were from Scharlau (Spain) or Sigma (USA) with an analytical grade, and were applied as received. Deionized water was employed for solutions preparation.

2.2. Oligonucleotide sequences

An oligonucleotide sequence (probe oligonucleotide, PO) was selected by Primer3 and the search tool of NCBI BLAST nucleotide based on the submitted GenBank sequence of AB678348.1 of *L. infantum* genome (Iranian Standard strain MCAN/IR/97/LON490, isolate: IranJWinf) [31]. PO was evaluated for shared oligonucleotide sequences and any homology of non-*L. infantum* species by BLAST of NCBI. Also, the melting point of PO was checked to be in a narrow temperature values by the Oligo software. Possibility of secondary structures and self-dimer formation of the PO sequence was checked as well by the mfold software [32]. PO had 26 bases and was thiolated from 5' end with six -CH_2- spacers. A target oligonucleotide (TO) sequence complementary with PO was also selected. The PO and TO sequences are reported in Table 1.

Table 1
The oligonucleotide sequences employed in this study.

Name	Oligonucleotide sequence (5′ to 3′)
PO	SH-$(CH_2)_6$-TTTTTTTTTTGTAATGTTACCCGATAGAAGTCTCGT
TO	ACGAGACTTCTATCGGGTAACATTAC
Forward PCR primer	CCACCCGGCCCTATTTTACA
Reverse PCR primer	GGCTGAAGCCTGTTAGTGGT
1-mis TO	**T**CGAGACTTCTATCGGGTAACATTAC
2-mis TO	**TG**CAGACTTCTATCGGGTAACATTAC
3-mis TO	**TGC**AGACTTCTATCGGGTAACATTAC
non TO	**AACCC**ACT**AAAGCGTCACCCAACACT**

PO: probe oligonucleotide.
TO: target oligonucleotide.
1-mis TO: a target oligonucleotide with one mismatched base, compared to TO.
2-mis TO: a target oligonucleotide with two mismatched bases, compared to TO.
3-mis TO: a target oligonucleotide with three mismatched bases, compared to TO.

Clinical samples assayed in this study were firstly confirmed by gel-electrophoresis followed by PCR for diagnosis of the parasite species. For PCR, the primers had sequences that were reported in Table 1. PCR was done by a thermal cycler from Bio-Rad T100 (USA).

For evaluation of the selectivity of the genosensor, one- (1-mis TO), two- (2-mis TO) and three-base mismatched oligonucleotides (3-mis TO) were assayed by the genosensor with sequences reported in Table 1. All the DNA sequences employed in this study were obtained from Cinaclon Co. (Iran). All these oligonucleotides were dissolved in a tris-HCl buffer solution (20 mmol L^{-1}, pH 7.4, denoted as Tris), and stored at -20 °C. Determination of DNA concentration of the samples was performed by a NanoDrop™ Lite Spectrophotometer (USA).

2.3. Electrochemical measurements

Electrochemical experiments were performed using a μ-Autolab potentiostat/galvanostat (the Netherlands) controlled by GPES and FRA softwares. Electrochemical analyses were performed using a three-electrode set-up composed of a platinum (Pt) rod counter electrode, a Pt disk electrode-covered CSN, or the genosensor as the working electrode (2 mm of diameter or 0.0314 cm^2 of geometric surface area), and an Ag/AgCl/3 mol L^{-1} KCl reference electrode. Electrochemical impedance spectra were recorded in Tris at open circuit potential as dc-offset in a frequency range of 50 kHz–100 mHz with an ac-amplitude of 10 mV. All the electrochemical measurements were performed at room temperature.

2.4. Preparation of the Pt disk electrode-covered CSN and characterization

The Pt disk electrode was firstly polished to a mirror-finished with alumina powder. The electrode was then washed with deionized water and cleaned ultrasonically in a mixture of ethanol:water (3:1 V/V) to remove alumina particles that might be attached on the surface. Deposition of CSN was performed in two steps. Firstly, a clean Pt disk electrode was immersed into a 0.1 mol L^{-1} $Cd(NO_3)_2$, and a constant potential of -1.2 V was applied to deposit a layer of $Cd(OH)_2$ on the surface. Then, the prepared $Cd(OH)_2$ thin film was dipped into a 0.1 mol L^{-1} aqueous solution of Na_2S and left for 60 min. During this time, $Cd(OH)_2$ was derivatized to CSN. Morphological analysis of CSN was performed using field emission scanning electron microscopy (FESEM) by a TESCAN Mira 3-XMU (Czech Republic) equipped with energy-dispersive X-ray (EDX) spectroscopy.

2.5. Immobilization of PO and fabrication of the genosensor

PO was pretreated to break the preformed S-S bonds. 10 μL of a solution containing 10 mmol L^{-1} sodium acetate, pH 5.2 and 500 mmol L^{-1} dithiothreitol (DTT) was added to a 10 μmol L^{-1} solution of PO, mixed and placed at ambient temperature for ~30 min. Excess amount DTT was then extracted with ethyl acetate.

PO immobilization on the Pt electrode-covered CSN was performed at an optimized time. For the optimization, open-circuit potential (OCP) was continuously measured as the immobilization of PO progressed. For this experiment, platinum screen-printed electrode from DropSens (Spain) covered by CSN was employed. A 10 μmol L^{-1} solution of PO was carefully dropped on the screen-printed electrode and kept refrigerated at 4 °C wherein OCP values were recorded by a Mastech multimeter (China).

Immobilization of PO on the Pt electrode-covered CSN was carried out by dropping 10 μL of the PO solution on the electrode surface and keeping it at 4 °C for the optimized immobilization time. Then, the electrode was washed with deionized water, and then 1.0 mmol L^{-1} 6-mercapto-1-hexanol was dropped on the electrode for 30 min. 6-mercapto-1-hexanol was also immobilized on the surface of Pt electrode-covered CSN to block the remaining sites on the surface not covered by PO, and induced formation of a monolayer of well-aligned PO. After washing with deionized water, the genosensor was ready to use.

2.6. Evaluation of the genosensor

The genosensor was hybridized with different concentrations of TO of 1.0×10^{-14} to 1.0×10^{-6} mol L^{-1} by incubation at 37 °C for a fixed time of 40 min [33]. The genosensor was then washed with deionized water and transferred into the electrochemical cell for impedimetric measurements.

The reproducibility of genosensor fabrication was checked by manufacturing the genosensor at different days. A previously fabricated genosensor was cleaned with Piranha solution to remove the organics from the surface followed by re-preparation of the Pt disk electrode-covered CSN, immobilization of PO, and recording a Nyquist diagram in Tris, as described in section 2.2. These steps were repeated five times and impedance spectra for the repeating fabrication were measured.

To check the genosensor regeneration ability, a Nyquist diagram was firstly measured using a newly fabricated genosensor. It was then hybridized with a 1.0×10^{-10} mol L^{-1} solution of TO and a Nyquist diagram war recorded. After this, the genosensor was placed in deionized water at 95 °C to release the hybridized TO, and a Nyquist diagram was recorded. The genosensor was re-hybridized again with similar TO concentration and a Nyquist diagram was measured. These steps were repeated five times.

The selectivity of the genosensor was inspected upon hybridization with four target oligonucleotides of mismatched base(s) (Table 1) at similar concentration of 1.0×10^{-10} mol L^{-1}, and Nyquist diagrams were recorded for each sequence. In addition, genomic DNA from *Leishmania tropica* (*L. tropica*) and *Leishmania major* (*L. major*) parasites was extracted and analyzed with the genosensor.

To examine the stability of the genosensor, we hybridized it with TO of 1.0×10^{-10} mol L^{-1}, and Nyquist diagrams were then measured in consecutive days. When it was not used, the genosensor was stored in Tris at 4 °C. Before analysis of the clinical samples, standard assays were done on the genome. The genomic samples of different concentrations in a range of 5–50 ng μL^{-1} were placed at 95 °C for 5 min followed by immediate cooling to break the DNA double strand. Then, the samples were placed on the genosensor surface and the corresponding Nyquist diagrams were measured. A calibration plot was afterward plotted to judge the genosensor ability for genomic DNA detection.

2.7. Parasite culture

The cryopreserved *L. infantum* (MCAN/IR/96/LON49), *Leishmania tropica* (MHOM/IR/02/Mash10) and *Leishmania major* (MRHO/IR/75/ER) were prepared from Tehran University of Medical Sciences, and cultured at 24 °C in RPMI 1640 medium containing 10% (V/V) heat-inactivated fetal bovine serum (Gibco) and 1% pen-strep (Sigma). A promastigotes parasite count of 1×10^7 mL^{-1} using a Neubauer chamber was handled. The culture medium was removed by centrifugation, around 10^7 phase promastigotes of the isolates were collected, washed with 50 mmol L^{-1} phosphate buffer saline (0.7% NaCl), pH = 7.0, and then re-dispersed in a buffer containing 0.5 mol L^{-1} EDTA, 5 mol L^{-1} NaCl, 1 mol L^{-1} Tris buffer, pH = 8.0 (the NET buffer).

Lysis of the parasite cells was performed at 56 °C, using a mixture of 100 mg mL^{-1} proteinase K and 1% sodium dodecyl sulfate for 4 h. The lyzed cells were treated by a DNA extraction kit according to the manufacturer's instructions. Concentration of parasitic DNA in the samples was measured, using a NanoDrop 2000c (Thermo Scientific, USA).

2.8. Clinical samples analysis

Applicability and suitability of the genosensor for analysis of the parasite in clinical samples were evaluated by analysis of one human specimen and five buffy coat specimens acquired from dogs with cutaneous lesions. Infection of these samples with *L. infantum* was already confirmed by gel-electrophoresis followed by PCR. Genome was extracted from these samples using a DNA extraction kit according to the manufacturer's instructions. The extracted DNA was directly analyzed by the genosensor without any pretreatment including amplification by PCR.

3. Results and discussion

Surface morphology of CSN was firstly assessed by FESEM, and the corresponding images are presented in Fig. 1A and B. Relative regular dendrites of cadmium sulfide were formed on the surface. The dendrites were sheets of different length of 0.4–2.1 μm with an average thickness of 67.3 ± 19.0 nm (n = 50). These nanosheets make cadmium sulfide more accessible for the next step of PO immobilization. Fig. 1C shows an EDX spectrum of CSN representing peaks related to its elemental composition accompanied by signals related to the underlying Pt disk electrode. The spectrum confirmed the high chemical purity of CSN.

To follow the progression of PO immobilization on the CSN surface and obtaining its optimized time, we measured the changes in OCP. Fig. 2 shows changes in the OCP value upon immobilization of PO on the CSN surface. Three clear different trends in the OCP changes are observed. An initial positive shift in the OCP values (< 280 s) was followed by a gradual and deep negative shift (> 280 s and < 3300 s) and further positive shift at longer times (> 3300 s). At times longer than 8000 s, positive changes in OCP values slowed down and reached a relatively steady value. This behavior was highly reproducible. As a rule, OCP value is principally determined by the electron exchange between redox species in the solution and the electrode surface that pin the electrode Fermi level. Further OCP changes indicate the entity of charge accumulation at a surface. The initial positive shift of OCP is related to the double layer formation and arrangement, and equilibration. Further negative OCP shift indicates attachment of thiol functional group of PO into CSN surface, according to the following reaction:

$$CSN(Cd^{2+}S^{2-}) + SH-PO \rightarrow CSN(Cd^{2+}S^{2-})S^{-}-PO + H^{+} \quad (1)$$

The net negative charge of PO arising from the DNA sugar-phosphate backbone is an alternative of negative change in OCP during PO attachment into CSN surface. At longer times (of > 3300 s), electron

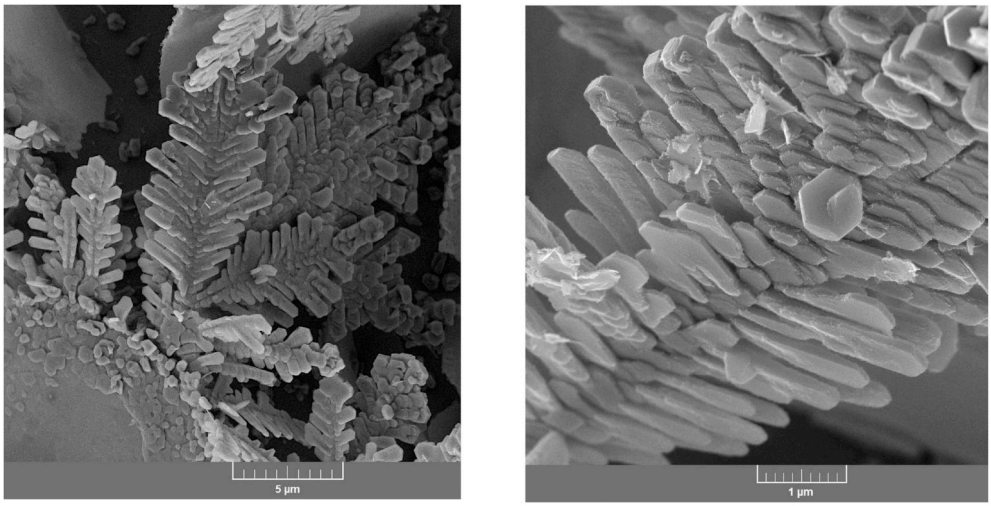

Fig. 1. FESEM images at two different magnifications (A, B) and an EDX spectrum (C) of CSN.

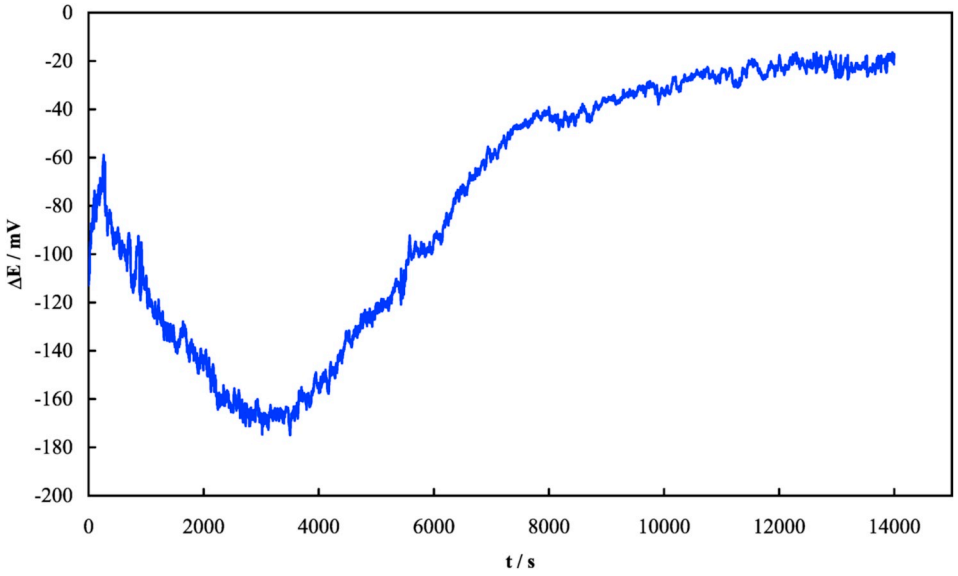

Fig. 2. Changes in OCP upon immobilization of PO on the CSN surface.

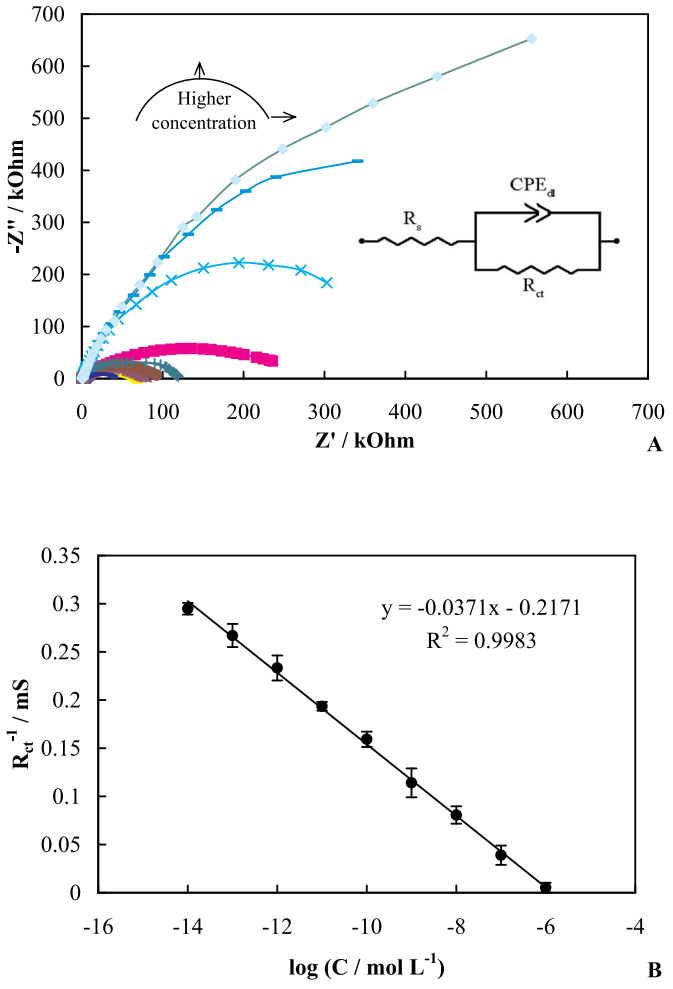

Fig. 3. Nyquist diagrams recorded before and after hybridization of the genosensor with different concentrations of TO of 1.0×10^{-14}, 1.0×10^{-13}, 1.0×10^{-12}, 1.0×10^{-11}, 1.0×10^{-10}, 1.0×10^{-9}, 1.0×10^{-8}, 1.0×10^{-7} and 1.0×10^{-6} mol L^{-1} (A), an equivalent electrical circuit compatible for the Nyquist diagrams (A, inset), and dependency of the charge transfer resistance values on the TO concentration (B).

transfer from CSN into hydronium ions via a partial oxidative reaction of sulfide occurs:

$$CSN(Cd^{2+}S^{2-})S^{-} - PO + H^{+} \rightarrow CSN(Cd^{2+}S^{-} - S^{-}) - PO + \tfrac{1}{2} H_2 \quad (2)$$

and positive shift in OCP takes place. Based on the results, the optimum immobilization time of PO on the CSN surface was selected as 3.9 h, and this time was employed for preparation of the genosensor throughout this study.

The genosensor was incubated for 40 min [33] with different concentrations of TO at 37 °C, so that the hybridization process between the strands occurs. Fig. 3A represents Nyquist diagrams recorded after and before hybridization of the genosensor with different TO concentrations. The impedance responses simply comprised one depressed semicircle related to the charge transfer process across the Pt/CSN/electrolyte interface. Upon hybridization, the total impedance of the genosensor increased in a concentration dependent manner. The Nyquist diagrams were characterized with the equivalent circuit shown in Fig. 3A, inset. In this circuit, R_{ct}, CPE_{dl} and R_s represent charge transfer resistance, a constant phase element describing the double layer capacitance and the solution ohmic resistance, respectively. CPE_{dl} characterized the capacitive semicircle in the Nyquist plot to be depressed, instead of a perfect capacitor, as reported elsewhere [9], arising from the roughening of the genosensor surface (from CSN morphology). The

Table 2
A comparison between various detection methods of *L. infantum*.

Detection method	Nanomaterial employed	Linear range	DL	Sensitivity	Reference
Electrochemical impedance	Carbon Nanotubes	0.1–98.3 fg μL^{-1}	15 fmol L^{-1}	–	[30]
Electrochemical impedance	Gold nanoparticles	0.01 pg mL^{-1} - 10 ng mL^{-1}	–	–	[24]
Surface plasmon resonance immunosensing	Gold nanoparticles	1–300 nmol L^{-1}	0.41 nmol L^{-1}	–	[35]
PCR enzyme-linked immunosorbent assay	–	–	50-100 promastigotes	1 fg	[36]
PCR enzyme-linked immunosorbent assay	–	0.07–700 fg	0.07 fg	100%	[37]
Electrochemical DNA sensor[a]	Non-spherical gold nanoparticles	10 amol L^{-1} - 0.1 nmol L^{-1}	0.2 amol L^{-1}	-0.1194 μA/[log (C^{b}/mol L^{-1})]	[38]
Electrochemical DNA sensor[c]	Non-spherical gold nanoparticles	15–50 ng μL^{-1}	9 ng μL^{-1}	-2.4432 μA/[log (C^{d}/ng μL^{-1})]	[38]
Impedimetric genosensor[a]	Cadmium sulfide nanosheets	10 fmol L^{-1} - 1.0 μmol L^{-1}	0.81 fmol L^{-1}	-0.0371 mS/[log (C^{b}/mol L^{-1})]	This srudy
Impedimetric genosensor[c]	Cadmium sulfide nanosheets	5–50 ng μL^{-1}	1.2 ng μL^{-1}	-0.0521 mS/[log (C^{d}/ng μL^{-1})]	This srudy

[a] For TO detection.
[b] Concentration of TO in mol L^{-1}.
[c] For detection of genomic DNA.
[d] Concentration of genomic DNA in ng μL^{-1}.

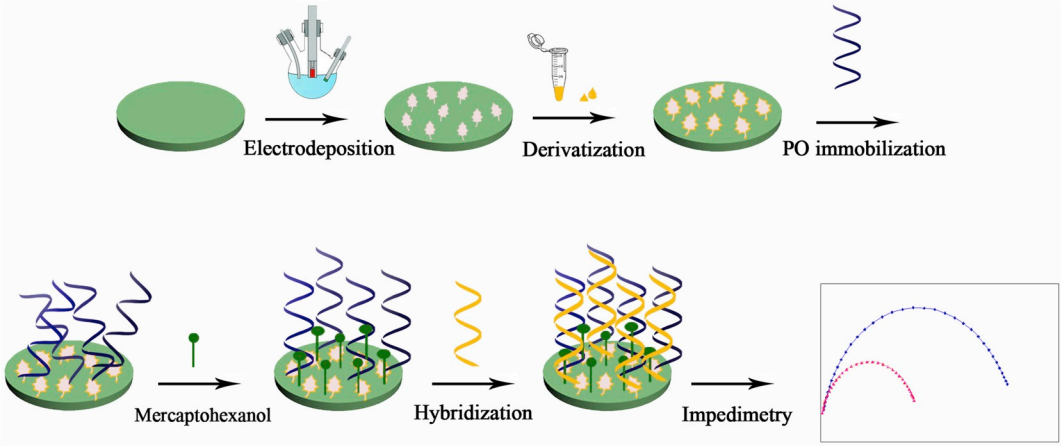

Scheme 1. The fabrication procedures and signal generation mechanism of the genosensor.

equivalent circuit was fitted on the Nyquist diagrams, and the dependency of the charge transfer resistance values on the TO concentration is shown in Fig. 3B (the values of the circuit elements are presented in Supplementary material S1). The impedimetric response of the genosensor had a linear relation of inverse of charge transfer resistance on the logarithm of TO concentration in a dynamic range of 1.0×10^{-14} to 1.0×10^{-6} mol L^{-1}. A regression equation was obtained as R_{ct}^{-1} [mS] = -(0.0371 ± 0.0006) log (C [/mol L^{-1}]) - (0.2171 ± 0.0060) [mS], R^2 = 0.9983. For calculation of detection limit (DL) of the genosensor to quantify TO, Nyquist diagrams were firstly recorded, using the genosensor in the absence of TO to obtain the standard deviation (SD_0) of the (inverse) of charge transfer resistance of the blank signal. Then, using the slope of the line in Fig. 3B and the relation (R_{ct}^{-1} - 3 × SD_0) as the LD signal (considering the genosensor is a signal-off type), LD was attained to be 0.81 fmol L^{-1} (equal to 6.5 fg mL^{-1}). This LD value is lower than the other reported impedimetric methods [24,30] and comparable with some others. Different detection methods of *L. infantum* were compared in Table 2. The fabrication procedures and signal generation mechanism are also shown in Scheme 1.

Reproducibility of the genosensor fabrication was investigated by recording Nyquist diagrams using five fabricated genosensors, as shown in Fig. 4 (the values of the circuit elements are presented in Supplementary material S2). Changes in the charge transfer resistance values had a relative standard deviation (RSD) of 6.2%, indicating a very good

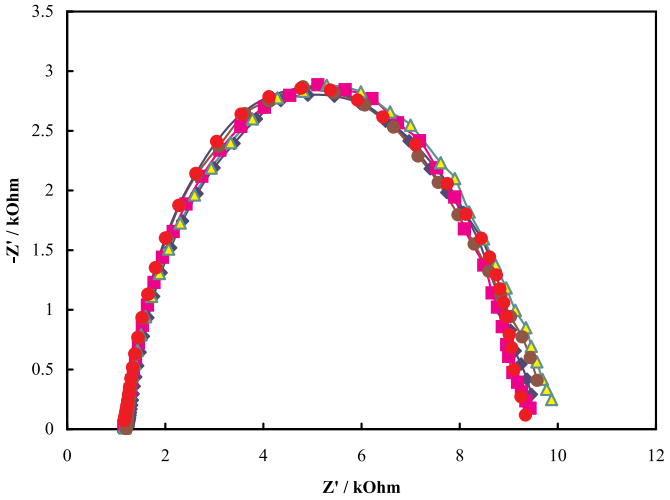

Fig. 4. Nyquist diagrams recorded using five fabricated genosensors (without hybridization with TO) to check the reproducibility of the genosensor fabrication.

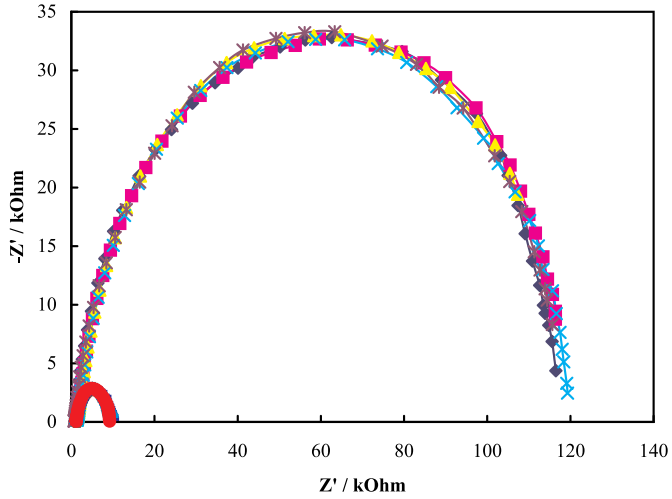

Fig. 5. Nyquist diagrams recorded using the genosensor upon five hybridization/dehybridization cycles with/from 1.0×10^{-10} mol L^{-1} TO.

reproducibility of genosensor fabrication.

Regeneration of the genosensor was checked by recording Nyquist diagrams before and after five cycles of hybridization/dehybridization of the genosensor with/from TO. Fig. 5 shows Nyquist diagrams recorded upon hybridization/dehybridization with/from TO (the values of the circuit elements are presented in Supplementary material S3). The genosensor represented RSD values for charge transfer resistances of 4.6 and 3.8% for hybridization and dehybridization cycles, respectively. These indicate a very good regeneration ability of the genosensor.

Selectivity of the genosensor was evaluated upon hybridization with four base-mismatched oligonucleotides of 1-mis TO, 2-mis TO, 3-mis TO and non TO at the same concentrations, and the related Nyquist diagrams are shown in Fig. 6 (the values of the circuit elements are presented in Supplementary material S4). The values of charge transfer resistance were changed in a manner of TO > 1-mis TO > 2-mis TO > 3-mis TO > non TO ≈ genosensor. Quantitatively, if hybridization of the genosensor with TO is assumed to be 100%, its hybridization was estimated to be 75, 48, 20 and 0.6%, for 1-mis TO, 2-mis TO, 3-mis TO and non TO, respectively. These findings indicated that the genosensor can discriminate the mismatched sequences.

To check the stability of the genosensor, we recorded the Nyquist diagrams in different consecutive days after hybridization with 1.0×10^{-10} mol L^{-1} of TO. Fig. 7 shows the changes in the values of charge transfer resistance with time, indicating that the genosensor had

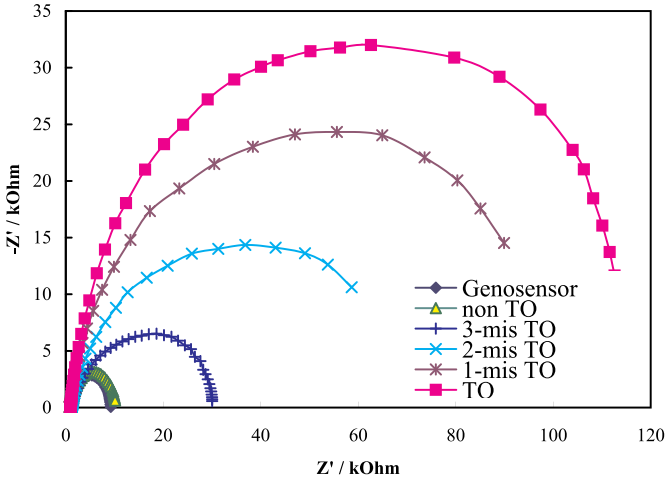

Fig. 6. Nyquist diagrams recorded before and after hybridization of the genosensor with 1-mis TO, 2-mis TO, 3-mis TO and non TO of 1.0 × 10^{-10} mol L^{-1}.

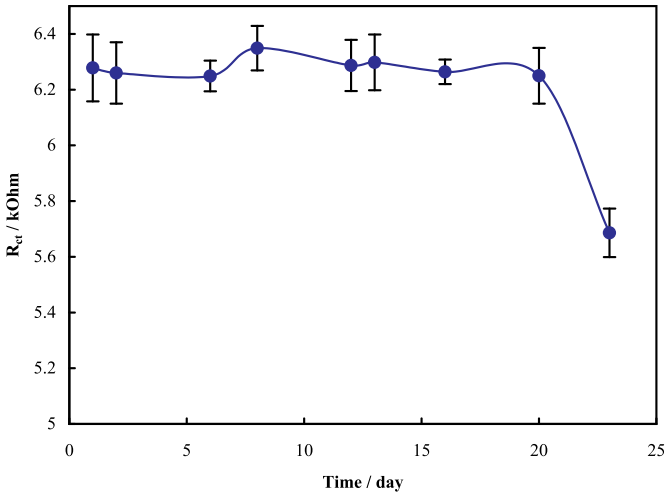

Fig. 7. Changes in the values of charge transfer resistance with storage time of the genosensor.

a relatively constant charge transfer resistance for at least 20 days. This time was then considered as the storage time of the genosensor.

The repeatability and reproducibility of the genosensor were deduced by independent determination of three concentrations of TO in one or three days to evaluate the intra-day or inter-day assays, respectively. The obtained results are demonstrated in Table 3. A 1.0 × 10^{-10} mol L^{-1} of TO was also determined by recording three Nyquist diagrams by a single genosensor. A RSD value of 2.77% was obtained for these determinations.

Impedimetric responses of the genosensor toward *L. infantum* genomic DNA were measured. The genosensor was incubated for 40 min [33] with different concentrations of genomic (single stranded) DNA at 37 °C, and the recorded Nyquist diagrams are displayed in Fig. 8A. The signature of these Nyquist diagrams is quite similar to those recorded for TO (Fig. 3A), comprising one depressed capacitive

Table 3
Precision (n = 3) for assay three concentrations of TO by the genosensor.

TO/mol L^{-1}	RSD% (intra-day assay)	RSD% (inter-day assay)
1.0 × 10^{-8}	2.96	3.18
1.0 × 10^{-10}	1.17	4.65
1.0 × 10^{-13}	3.33	3.85

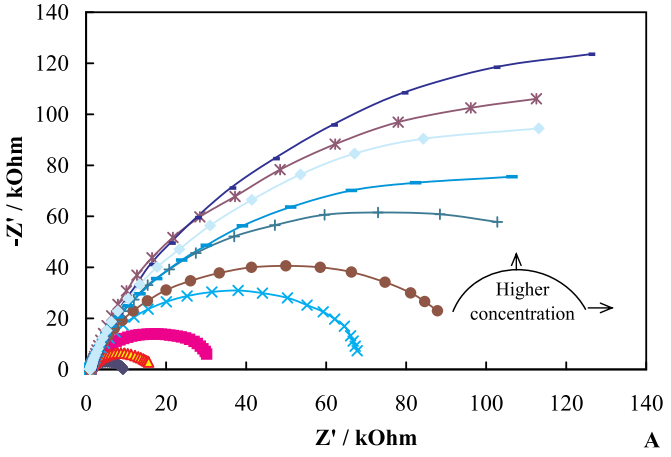

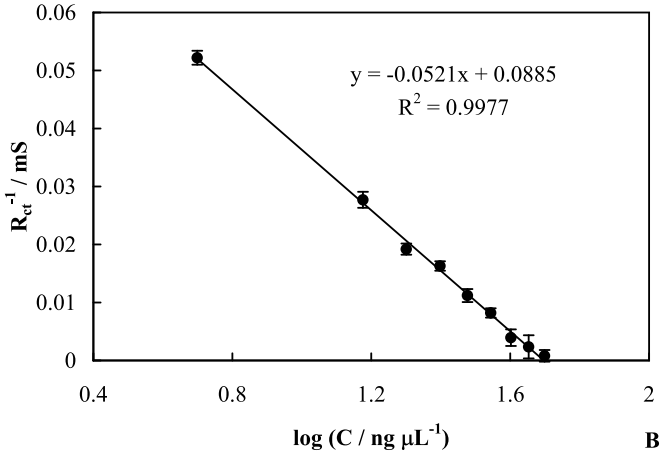

Fig. 8. Nyquist diagrams recorded before and after hybridization of the genosensor with different concentrations of genomic DNA of 5, 15, 20, 25, 30, 35, 40, 45 and 50 ng μL^{-1} (A), and dependency of the charge transfer resistance values on the genomic DNA concentration (B).

semicircle. Similarly, hybridization of genomic DNA with the genosensor increased the total impedance and charge transfer resistance, and he Nyquist diagrams were characterized with the equivalent circuit shown in Fig. 3A, inset. The equivalent circuit was fitted on the Nyquist diagrams, and the dependency of the charge transfer resistance values on concentration of genomic DNA is shown in Fig. 8B (the values of the circuit elements are presented in Supplementary material S5). The impedimetric signals depended on the logarithm of the concentration of genomic DNA in a linear range of 5–50 ng μL^{-1} with a regression equation of R_{ct}^{-1} [mS] = -(0.0521 ± 0.0009) log (C [/ng μL^{-1}]) + (0.0885 ± 0.0014) [mS], R^2 = 0.9977. DL of the genosensor to quantify the genome was also acquired to be 1.2 ng μL^{-1}. In addition, genomic DNA from *L. major* and *L. tropica* were detected using the genosensor for which the recorded Nyquist diagrams are presented in Fig. 9 (the values of the circuit elements are presented in Supplementary material S6). The results pointed out that the genosensor did not have noticeable responses to *L. Major* and *L. tropica*, indicating the good selectivity of the genosensor toward *L. infantum*.

To verify the genosensor applicability for parasite detection in clinical samples, genomic DNA was extracted from some human and canine specimens and firstly assayed to confirm being infected with the parasite by gel-electrophoresis followed by PCR. Then, the genomic DNA was directly (without amplification by PCR) analyzes by the genosensor. Quantitation limit (QL) of a sensing device is presented as a concentration that generates a signal of 10 × SD_0 [34].

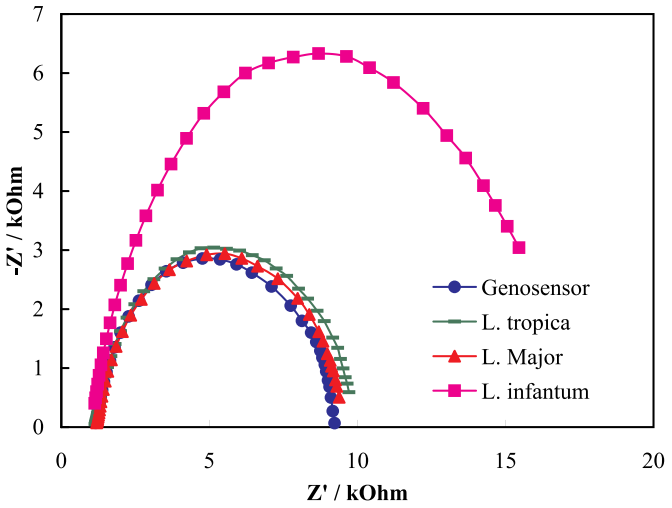

Fig. 9. Nyquist diagrams recorded before and after hybridization of the genosensor with 15 ng μL^{-1} genomic DNA from *L. major*, *L. tropica* ad *L. infantum*.

Correspondingly, any impedimetric signal greater than 10 × SD_0 was considered being positive. The results obtained for the clinical samples assay are presented in Supplementary material S7, indicating that the genosensor results were in agreement with those already obtained by gel-electrophoresis followed by PCR. These results, therefore, confirmed the genosensor applicability to analyze clinical samples.

4. Conclusion

A specific oligonucleotide sequence was designed from gene sequence of *L. infantum* followed by immobilization on the CSN surface through self-assembling to fabricate the genosensor. PO self-assembling on the CSN surface followed a multiple process with different time scales. Various oligonucleotide sequences as well as the parasite genomic DNA were hybridized with the immobilized sequence, and the quantity of hybridization process was followed by impedimetric measurements without any redox marker, tag or label. The designed genosensor showed high calibration sensitivities and low values of DL for both synthetic TO and genomic DNA, and can discriminate base-mismatched sequences with a high selectivity. The genosensor was applied for diagnosis of clinical samples, and the results revealed successful suitability for the parasite detection in practical samples.

CRediT authorship contribution statement

R. Nazari-Vanani: Data curation, Formal analysis, Methodology, Writing - review & editing. **H. Heli:** Conceptualization, Formal analysis, Resources, Validation, Writing - review & editing. **N. Sattarahmady:** Conceptualization, Formal analysis, Investigation, Project administration, Resources, Writing - review & editing.

Declaration of competing interest

There is no Conflict of interest.

Acknowledgments

Research reported in this publication was supported by Elite Researcher Grant Committee under award number [976959] from the National Institute for Medical Research Development (NIMAD), Tehran, Iran.

Appendix A. Supplementary data

Supplementary data to this article can be found online at https://doi.org/10.1016/j.talanta.2020.121080.

References

[1] H.C. Hoch, L.W. Jelinski, H.G. Craighead, Nanofabrication and Biosystems: Integrating Materials Science, Engineering, and Biology, Cambridge University Press, 1996.
[2] R. Nazari-Vanani, N. Sattarahmady, H. Yadegari, H. Heli, A novel and ultrasensitive electrochemical DNA biosensor based on an ice crystals-like gold nanostructure for the detection of Enterococcus faecalis gene sequence, Colloids Surf., B 185 (2018) 69–76.
[3] A. Rahi, N. Sattarahmady, H. Heli, Zepto-molar electrochemical detection of Brucella genome based on gold nanoribbons covered by gold nanoblooms, Sci. Rep. 5 (2015) 18060.
[4] L. Gorton (Ed.), Biosensors and Modern Biospecific Analytical Techniques, Elsevier Science, 2005.
[5] F.R.R. Teles, L.P. Fonseca, Trends in DNA biosensors, Talanta 77 (2008) 606–623.
[6] A.P. De Silva, T.S. Moody, G.D. Wright, Fluorescent PET (Photoinduced Electron Transfer) sensors as potent analytical tools, Analyst 134 (2009) 2385–2393.
[7] N. Sattarahmady, H. Heli, R.D. Vais, A flower-like nickel oxide nanostructure: synthesis and application for choline sensing, Talanta 119 (2014) 207–213.
[8] H. Heli, S. Majdi, A. Jabbari, N. Sattarahmady, A.A. Moosavi-Movahedi, Electrooxidation of dextromethorphan on a carbon nanotube–carbon microparticle–ionic liquid composite: applied to determination in pharmaceutical forms, J. Solid State Electrochem. 14 (2010) 1515–1523.
[9] N. Sattarahmady, H. Heli, A non-enzymatic amperometric sensor for glucose based on cobalt oxide nanoparticles, J. Exp. Nanosci. 7 (2012) 529–546.
[10] A. Rahi, N. Sattarahmady, R.D. Vais, H. Heli, Sonoelectrodeposition of gold nanorods at a gold surface–Application for electrocatalytic reduction and determination of nitrofurazone, Sensor. Actuator. B 210 (2015) 96–102.
[11] J. Arbiol, Q. Xiong (Eds.), Semiconductor Nanowires: Materials, Synthesis, Characterization and Applications, Woodhead Publishing, 2015.
[12] G.H. Zhu, K. Tomsia, H. Yu, E.M. Goldys, Chemically binding Eu3+ onto CdS semiconductor nanoparticle surface, Chin. Chem. Lett. 18 (2007) 581–584.
[13] Z. Atay, T. Biver, A. Corti, N. Eltugral, E. Lorenzini, M. Masini, et al., Non-covalent interactions of cadmium sulphide and gold nanoparticles with DNA, J. Nanoparticle Res. 12 (2010) 2241–2253.
[14] K.B.A. Ahmed, M.R.C. Raja, S.K. Mahapatra, V. Anbazhagan, Interaction of cadmium sulfide quantum dots with jacalin for specific recognition of cancer cells, J. Lumin. 182 (2017) 283–288.
[15] U.S. Jeng, Y.-S. Sun, H.-Y. Lee, C.-H. Hsu, K.S. Liang, S.-W. Yeh, et al., Binding effect of surface-modified cadmium sulfide on the microstructure of PS-b-PEO block copolymers, Macromolecules 37 (2004) 4617–4622.
[16] F. Wang, S. Hu, Electrochemical sensors based on metal and semiconductor nanoparticles, Microchimica Acta 165 (2009) 1–22.
[17] D. Steverding, The history of leishmaniasis, Parasites Vectors 10 (2017) 82.
[18] R.S. Gomes, M.V.T. Silva, J.C. dos Santos, C. van Linge, J.M. Reis, M.M. Teixeira, et al., Human interleukin-32γ plays a protective role in an experimental model of Visceral Leishmaniasis in mice, Infect. Immun. 86 (2018) 00796.
[19] C. Maia, L. Campino, Biomarkers associated with Leishmania infantum exposure, infection, and disease in dogs, Frontiers Cell. Infect. Microbiol. 8 (2018) 302.
[20] R.C. Spear, Review of "Mathematical Models for Neglected Tropical Diseases: Essential Tools for Control and Elimination, Part B" Edited by Maria-Gloria Basanez and Roy M. Anderson, Parasites Vectors vol. 10, (2017) 38.
[21] M. Antoniou, C. Doulgerakis, F. Pratlong, J.P. Dedet, Y. Tselentis, Short report: treatment failure due to mixed infection by different strains of the parasite Leishmania infantum, Am. Soc. Tropical Med. Hygiene 71 (2004) 71–72.
[22] F. Chappuis, S. Sundar, A. Hailu, H. Ghalib, S. Rijal, R.W. Peeling, et al., Visceral leishmaniasis: what are the needs for diagnosis, treatment and control? Nat. Rev. Microbiol. 5 (2007) 873–882.
[23] S. Sundar, M. Rai, Laboratory diagnosis of visceral leishmaniasis, Clin. Vaccine Immunol. 9 (2002) 951–958.
[24] M.F.K.d.S. Garcia, C.A.S. Andrade, C.P. de Melo, D.S. Gomes, L.G. Silva, R.V. Dias, et al., Impedimetric sensor for Leishmania infantum genome based on gold nanoparticles dispersed in polyaniline matrix, J. Chem. Technol. Biotechnol. 91 (2016) 2810–2816.
[25] L. Solano-Gallego, A. Rodriguez-Cortes, M. Trotta, C. Zampieron, L. Razia, T. Furlanello, et al., Detection of Leishmania infantum DNA by fret-based real-time PCR in urine from dogs with natural clinical leishmaniosis, Vet. Parasitol. 147 (2007) 315–319.
[26] A.L. Carvalho Ferreira, V.M. Carregal, S. de Almeida Ferreira, R.S. Leite, A.S. de Andrade, Detection of Leishmania infantum in 4 different dog samples by real-time PCR and ITS-1 nested PCR, Diagn. Microbiol. Infect. Dis. 78 (2014) 418–421.
[27] F. Dantas-Torres, K.G. da Silva Sales, L. Gomes da Silva, D. Otranto, L.A. Figueredo, Leishmania-FAST15: a rapid, sensitive and low-cost real-time PCR assay for the detection of Leishmania infantum and Leishmania braziliensis kinetoplast DNA in canine blood samples, Mol. Cell. Probes 31 (2017) 65–69.
[28] D.E. Souto, J.V. Silva, H.R. Martins, A.B. Reis, R.C. Luz, L.T. Kubota, et al., Development of a label-free immunosensor based on surface plasmon resonance technique for the detection of anti-Leishmania infantum antibodies in canine serum, Biosens. Bioelectron. 46 (2013) 22–29.

[29] M.F. Persichetti, L. Solano-Gallego, A. Vullo, M. Masucci, P. Marty, P. Delaunay, et al., Diagnostic performance of ELISA, IFAT and Western blot for the detection of anti-Leishmania infantum antibodies in cats using a Bayesian analysis without a gold standard, Parasites Vectors 10 (2017) 119–126.
[30] I.A.M. Frias, C.A.S. Andrade, V.Q. Balbino, C.P. de Melo, Use of magnetically disentangled thiolated carbon nanotubes as a label-free impedimetric genosensor for detecting canine Leishmania spp. infection, Carbon 117 (2017) 33–40.
[31] S. Khademvatan, N. Neisi, S. Maraghi, J. Saki, Diagnosis and identification of Leishmania spp. from Giemsa-stained slides, by real-time PCR and melting curve analysis in south-west of Iran, Ann. Trop. Med. Parasitol. 105 (2011) 559–565.
[32] M. Zuker, Mfold web server for nucleic acid folding and hybridization prediction, Nucleic Acids Res. 31 (2003) 3406–3415.
[33] M. Negahdary, M. Behjati-Ardakani, N. Sattarahmady, H. Yadegari, H. Heli, Electrochemical aptasensing of human cardiac troponin I based on an array of gold nanodumbbells-Applied to early detection of myocardial infarction, Sensor. Actuator. B 252 (2017) 62–71.
[34] J.C. Miller, J.N. Miller, Significance Tests in Statistics for Analytical Chemistry, Ellis Horwood, Chichester, 1993.
[35] S.Y. Neto, D.E. P Souto, H.M. de Andrade, R.D.C. S Luz, L.T. Kubota, F.S. Damos, Visible LED light driven photoelectroanalytical detection of antibodies of visceral leishmaniasis based on electrodeposited CdS film sensitized with Au nanoparticles, Sensor. Actuator. B 256 (2018) 682–690.
[36] J. Martin-Sanchez, M.C. Lopez-Lopez, C. Acedo-Sanchez, J.J. Castro-Fajardo, J.A. Pineda, F. Morillas-Marquez, Diagnosis of infections with Leishmania infantum using PCR-ELISA, Parasitology 122 (2001) 607–615.
[37] F.A.C. Medeiros, L.I. Gomes, E. Oliveira, C.S.A. de Souza, M.V. Mourao, G.F. Cota, L.H.D. Marques, M. Carneiro, A. Rabello, Development and validation of a PCR-ELISA for the diagnosis of symptomatic and asymptomatic infection by Leishmania (Leishmania) infantum, J. Trop. Med. 2017 (2017) 1–10.
[38] R. Nazari-Vanani, N. Sattarahmady, H. Yadegari, N. Delshadi, G.R. Hatam, H. Heli, Electrochemical quantitation of Leishmania infantum based on detection of its kDNA genome and transduction of non-spherical gold nanoparticles, Anal. Chim. Acta 1041 (2018) 40–49.